PROCEEDINGS A

royalsocietypublishing.org/journal/rspa

Research

**Cite this article:** Dombroski A, Oakley K, Arcadia C, Nouraei F, Chen SL, Rose C, Rubenstein B, Rosenstein J, Reda S, Kim E. 2021 Implementing parallel arithmetic via acetylation and its application to chemical image processing. *Proc. R. Soc. A* 20200899. https://doi.org/10.1098/rspa.2020.0899

Received: 19 November 2020

Accepted: 30 March 2021

**Subject Areas:**
molecular computing, hybrid computing, image processing

**Keywords:**
chemical computing, linear operations, multiplication, image processing, acetylation

**Author for correspondence:**
Amanda Dombroski
e-mail: amanda_dombroski@alumni.brown.edu

Electronic supplementary material is available online at rs.figshare.com.

THE ROYAL SOCIETY PUBLISHING

# Implementing parallel arithmetic via acetylation and its application to chemical image processing

Amanda Dombroski, Kady Oakley, Christopher Arcadia, Farnaz Nouraei, Shui Ling Chen, Christopher Rose, Brenda Rubenstein, Jacob Rosenstein, Sherief Reda and Eunsuk Kim

Brown University, Providence, RI 02912, USA

AD, 0000-0003-2801-9558

Chemical mixtures can be leveraged to store large amounts of data in a highly compact form and have the potential for massive scalability due to the use of large-scale molecular libraries. With the parallelism that comes from having many species available, chemical-based memory can also provide the physical substrate for computation with increased throughput. Here, we represent non-binary matrices in chemical solutions and perform multiple matrix multiplications and additions, in parallel, using chemical reactions. As a case study, we demonstrate image processing, in which small greyscale images are encoded in chemical mixtures and kernel-based convolutions are performed using phenol acetylation reactions. In these experiments, we use the measured concentrations of reaction products (phenyl acetates) to reconstruct the output image. In addition, we establish the chemical criteria required to realize chemical image processing and validate reaction-based multiplication. Most importantly, this work shows that fundamental arithmetic operations can be reliably carried out with chemical reactions. Our approach could serve as a basis for developing more advanced chemical computing architectures.

## 1. Introduction

All living systems are capable of storing and processing chemical information, as they constantly perceive and respond to environmental signals. Biochemical reaction

networks can be exploited for digital molecular information storage and computing [1]. Often, these chemical and biological processes are orders of magnitude more space- and energy-efficient than modern electronic computers [2]. Recent forays into chemical-domain computing have generally centered around well-established biochemical reactions, such as DNA hybridization, where single strands of DNA can represent logic gates and be assembled into DNA-based logic circuits [3–7]. DNA strand displacement reactions have also been used as a model to illustrate computation of polynomial functions [8]. However, chemistry also provides a source of reactions suited for computation that offer significant advantages over biological computing. For instance, the Belousov–Zhabotinsky (BZ) reaction and other oscillating reactions display nonlinear chemical dynamics, which are reminiscent of behaviours observed in biological systems [9]. The BZ reaction has been used in time-delay chemical circuits [10] and other catalytic reactions have been incorporated into analogue and digital circuits by exploiting chemical logic gates [11–13].

Previously reported reaction-based models for computing primarily involved autocatalytic reactions and chemical reaction networks that made use of reaction–diffusion processes [9,14,15]. In our previous work, we presented a general framework for encoding and classification of images represented by chemical mixtures [16], where the binary pixels of input images were encoded by the presence, 1, or the absence, 0, of a chemical compound in a solution. The dot product operations required for image classification were carried out by weighted volumetric pooling with the final class determination readout via liquid chromatography. By using mixtures of non-reactive compounds, we were able to perform multiple classifications in parallel with the same number of volumetric multiply and accumulate operations as a single classification.

In this work, we propose a chemical-based computing system in which (i) the data operands are encoded chemically (e.g. using phenols) and superimposed into mixtures, and (ii) arithmetic operations are conducted on the operands in parallel using chemical reactions (e.g. acetylation), such that a single reaction type operates on multiple data values akin to single-instruction multiple data (SIMD) processors. To maximize computational throughput, we design a molecular encoding scheme with three key properties. First, we use the analogue concentration of molecular compounds to represent numerical values. Second, we strategically select molecular compounds that do not cross-react to superimpose them together to store multiple data values in a single molecular mixture. If $M$ denotes the identified molecular compounds, each with $Q$ levels of concentration, then we can encode $q = M\log_2 Q$ bits in an individual molecular mixture. Third, to ensure an accurate arithmetic implementation, we introduce additional reactants in the mixtures to ensure that the competition for the reactants by the acetylation kinetics leads to the desired arithmetic output. We showcase an implementation of our method on a parallel image processing application, where an image is chemically encoded, with $M = 4$, $Q = 8$, and parallelly processed with convolution kernels all *in chemico*.

We envision two potential applications for our system. First, our approach opens the possibility of intrinsic molecular computing directly in chemical and biochemical environments, eliminating the need for transducers and external processing. This approach will simplify soft robots and other devices that make decisions and actuate based on the chemical inputs they sense through seamless integration of these tasks. Second, our approach shows that it is possible to compute in parallel *in chemico*, where reactions occur *in situ*, eliminating the data transfer bottleneck between the main memory and the processor in von Neumann architectures. While our computational throughput is a far cry from that observed in modern digital processors, which have been successively improving for over 80 years, we can imagine a possibility in the future for molecular processors with high-throughput capabilities that have the capacity to execute operations on massive sets of data in parallel, potentially outperforming electronic processors for specific tasks [17].

Reaction-based arithmetic via phenol acetylation was used in two demonstrations of image processing. An image processing case study was performed which consisted of using one phenol to encode the greyscale input image data and the addition of equal amounts of acetic anhydride to apply an averaging kernel for processing. A parallel image processing case study was also

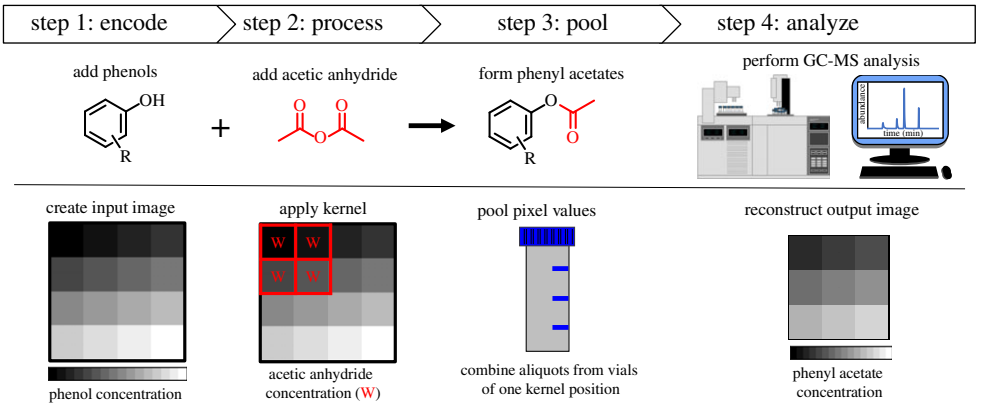


**Figure 1.** Overview of image processing using chemical reactions. Matrix multiplications for the 2 × 2-pixel convolution filter are performed with phenol acetylation reactions. In step 1, the 4 × 4-pixel greyscale input image is created using various concentrations of phenols (black), with darker pixel intensity representing lower concentrations of phenols and lighter pixel intensity representing higher concentrations of phenols. In step 2, the individual pixels of the input image are processed through a chemical transformation known as acetylation. This is performed by addition and reaction of phenols with a specified concentration, *W*, of acetic anhydride (red) as the kernel (red box) moves across the input image. In step 3, equal aliquots of the resulting phenyl acetate products (black and red) from the vials associated with one kernel position are pooled, resulting in an output image pixel. In step 4, these vials are analysed using Gas Chromatography-Mass Spectrometry (GC-MS) to obtain the output image pixel intensity, which is represented by phenyl acetate concentration. The output image is then reconstructed *in silico* from the measured concentrations of phenyl acetates. (Online version in colour.)

Q2

performed with four phenols to encode input image data using a partitioning technique that allows parallel acetylation reactions to represent matrix operations. This approach was used with a small greyscale image that was processed with a Gaussian kernel by additions of acetic anhydride that correspond to the various kernel weights. These image processing examples are discussed in greater detail in the following sections. Throughout this work, our chemical image processing pipeline consists of the following steps (figure 1):

1) Input images are encoded in concentrations of mutually, non-reactive phenol compounds, which represent the input image pixel intensity.
2) Phenol compounds are acetylated with acetic anhydride to represent matrix multiplication.
3) Equal aliquots from the resulting reaction mixtures are pooled to represent addition.
4) Concentrations of phenyl acetate reaction products are read out using standard analytical methods and represent output image pixel intensity.
5) Processed images are reconstructed based on these phenyl acetate measurements *in silico*.

Ultimately, these case studies provide the basis to perform more complex *in chemico* information processing and hint at the possibility of extending chemical computing beyond the applications presented here.

## 2. *In chemico* linear computation

### (a) Representing information in phenol concentrations

In conventional computers, data are represented using discrete voltages. In a chemical system, the concentration of a chemical compound can similarly be used to store information [8]. Since concentration is a continuous variable, it must be discretized to encode digital data, such that

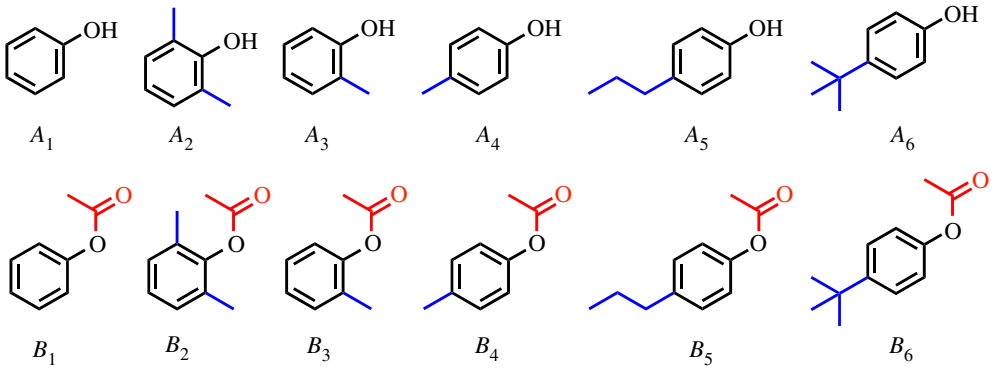


**Figure 2.** Structures of phenols and phenyl acetates. These phenolic compounds and their phenyl acetate products were used in the present work. $A_1$ and $A_2$, as well as their acetylation products, $B_1$ and $B_2$, were used in preliminary studies of reaction-based multiplication and the first demonstration of image processing on a small greyscale image. $A_1$, $A_3$, $A_4$, $A_5$ and $A_6$ and their respective phenyl acetate products, $B_1$, $B_3$, $B_4$, $B_5$ and $B_6$, were used in a second demonstration of parallel image processing via a partitioning method. (Online version in colour.)

the number of concentration levels depends on the number of bits used to represent the data. For example, defining $2^q$ levels of concentration corresponds to encoding the data in $q$ bits. In this work, we encode the three-bit or four-bit greyscale colour of a pixel with 8 or 16 levels of chemical concentration, respectively. The number of levels that can be used in a real experiment depends on the instruments used to write (liquid handler) and read (GC-MS) chemically encoded data. To encode image data in molecular concentrations, we employed two phenolic compounds, phenol, $A_1$, and 2,6-dimethylphenol, $A_2$ (figure 2, top), in our proof of concept studies used to validate reaction-based multiplication. These were also used in our image processing case study. Additionally, four substituted phenols, o-cresol, $A_3$, p-cresol, $A_4$, p-propylphenol, $A_5$, and p-tert-butylphenol, $A_6$ (figure 2, top), were used to store image data in our parallel image processing case study. The respective acetylation products of these phenols are phenyl acetate, $B_1$, 2,6-dimethylphenyl acetate, $B_2$, o-tolyl acetate, $B_3$, p-tolyl acetate, $B_4$, p-propylphenyl acetate, $B_5$ and p-tert-butylphenyl acetate, $B_6$ (figure 2, bottom).

Phenol compounds were selected to encode information based upon their favourable stoichiometry, or mole ratios, and reaction rates in preliminary experiments (electronic supplementary material, tables S1 and S2). The ability of phenols to undergo acetylation to completion results in conserved stoichiometry, which is necessary for performing arithmetic. Furthermore, a variety of different phenols can undergo acetylation simultaneously with similar reaction kinetics making parallel arithmetic possible.

## (b) Multiplication with acetylation

Acetylation is one of the most common and important reactions in organic chemistry. In cellular biology, acetylation performs co- and post-translational modification of proteins and is important for gene expression and cellular metabolism [18,19]. However, in traditional organic chemistry, acetylation is often used to protect a variety of functional groups, such as alcohols, amines, thiols, and phenols [20]. Phenol acetylation (figure 3, top) is often favoured by chemists as it is a rather robust reaction that can tolerate various substituted phenols as inputs and occurs under mild conditions [21]. When these attributes are coupled with agreeable kinetics, reaction parallelism and simultaneous computation can be achieved.

In the framework of reaction-based multiplication, the concentration of a phenol compound is used to encode input data. The multiplication product is determined by the concentration of the reaction product (phenyl acetate), which represents processed or output data. Assuming the

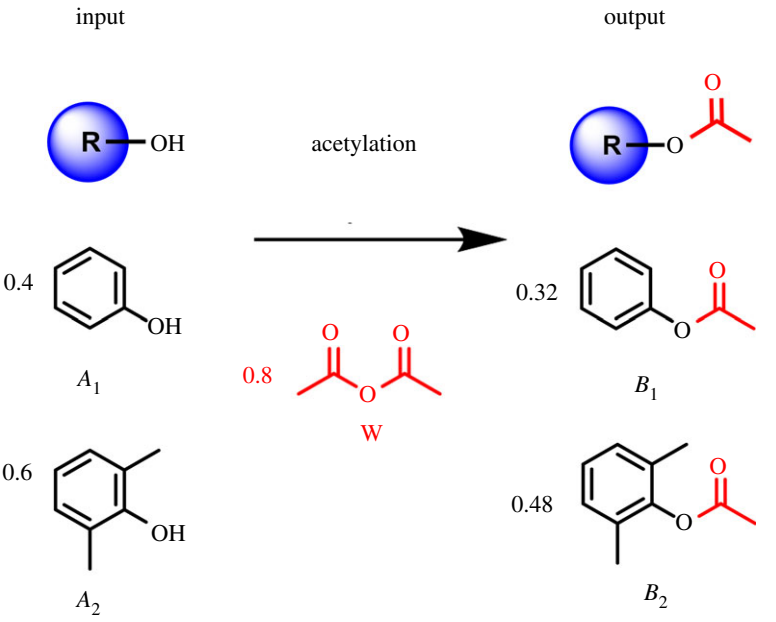


**Figure 3.** Phenol acetylation reaction scheme for reaction-based multiplication. A compound, such as a phenol, that contains a free hydroxyl group (black) undergoes acetylation by an acetylating reagent. During this chemical reaction, the hydrogen of the hydroxyl group is replaced by an ester known as an acetate (red). Phenol, $A_1$, and 2,6-dimethylphenol, $A_2$, are acetylated to phenyl acetate, $B_1$, and 2,6-dimethylphenyl acetate, $B_2$, using acetic anhydride, $W$. A multiplication operation occurs in the form of this reaction where phenols, multiplicands, and acetic anhydride, multiplier, react resulting in formation of phenyl acetate products in the amounts shown. Here, $W$ is in the range [0 . . . 1], and as result, the product is always less than or equal to the input. (Online version in colour.)

Q2

phenol acetylation reactions proceed to completion, they may be expressed as:

$$W + A_1 + A_2 \rightarrow B_1 + B_2, \tag{2.1}$$

where $A_1$ and $A_2$ are two phenol compounds present in a mixture, $W$ is the acetic anhydride acetylating reagent added to the mixture which initiates the chemical reaction, and $B_1$ and $B_2$ are the phenyl acetate products formed from reactions $W + A_1$ and $W + A_2$, respectively. Consequently, the following will also hold true and represents the output or multiplication product of each reaction:

$$[B_1]_f = \frac{[W]_o \cdot [A_1]_o}{[A_1]_o + [A_2]_o} \tag{2.2}$$

and

$$[B_2]_f = \frac{[W]_o \cdot [A_2]_o}{[A_1]_o + [A_2]_o}, \tag{2.3}$$

where $[.]_o$ is the initial reactant concentration and $[.]_f$ is the final product concentration in the mixture. In this context, the multiplicand is represented by the concentration of phenol compound, $A_2$, and the multiplier, $W$, is represented by the concentration of acetic anhydride or the common reactant. The mixture of $A_2$ and the auxiliary compound, $A_1$, remains inert until the addition of acetic anhydride. The addition of acetic anhydride results in two parallel acetylation reactions. Assuming the rates of these two reactions are similar, the proportion of $[W]_o$ reacting with $A_2$ will be determined by the ratio of the concentrations $[A_1]_o$ and $[A_2]_o$ in the mixture. After the reaction has occurred, the phenyl acetate product, $B_2$, is formed and represents multiplication of the two concentrations of $[A_2]_o$ and $[W]_o$. If the concentration of $[A_1]_o$ is selected such that $[A_1]_o + [A_2]_o = '1'$, where '1' is the maximum concentration, then $[B_2]_f$ gives the exact result for the

**Table 1.** Results of reaction-based multiplication with phenol acetylation. This table displays expected and measured stoichiometric equivalents for 2 phenols, phenol, $A_1$, and 2,6-dimethylphenol, $A_2$. The first column is the stoichiometric equation of the reaction, or the input, and the following four columns display the expected (left) and measured (right) stoichiometric amounts of the remaining unreacted phenols, $[A_1]$ and $[A_2]$, and the phenyl acetate products, $[B_1]$ and $[B_2]$, after addition of acetic anhydride, or the output. These measured stoichiometric equivalents are synonymous with concentration and found using relative GC peak area abundance.

| input | output (expected)\|(measured) | | | |
|---|---|---|---|---|
| reaction equation | $A_1$ | $A_2$ | $B_1$ | $B_2$ |
| $1 \times (0.5A_1 + 0.5A_2) \rightarrow 0.50B_1 + 0.50B_2$ | 0\|0[a] | 0\|0.08 | 0.50\|0.48 | 0.50\|0.44 |
| $1 \times (0.3A_1 + 0.7A_2) \rightarrow 0.30B_1 + 0.70B_2$ | 0\|0[a] | 0\|0.10 | 0.30\|0.24 | 0.70\|0.66 |
| $0.8 \times (0.4A_1 + 0.6A_2) \rightarrow 0.08\,A_1 + 0.12\,A_2 + 0.32B_1 + 0.48B_2$ | 0.08\|0.02 | 0.12\|0.19 | 0.32\|0.32 | 0.48\|0.47 |
| $0.5 \times (0.4A_1 + 0.6A_2) \rightarrow 0.20\,A_1 + 0.30\,A_2 + 0.20B_1 + 0.30B_2$ | 0.20\|0.07 | 0.30\|0.38 | 0.20\|0.24 | 0.30\|0.30 |
| $0.5 \times (0.6A_1 + 0.4A_2) \rightarrow 0.30\,A_1 + 0.20\,A_2 + 0.30B_1 + 0.20B_2$ | 0.30\|0.17 | 0.20\|0.17 | 0.30\|0.32 | 0.20\|0.17 |

[a]Not detectable.

multiplication. In computing systems, the number of bits associated with a data variable controls the maximum range of data; for example, an 8-bit system, which is typically used for storing greyscale pixel values, enables a representation of any integer value between 0 (black colour) and 255 (white colour). In our numerical representation system, '1' represents the maximum concentration which is associated with 255. That is, we normalize all values in the computational system by dividing by the maximum value, thereby leading to weights that are less than or equal to one. Since $W$ is in the range $[0 \ldots 1]$, the product is always less than or equal to the input. This scheme is reasonable for our image processing applications, where many kernels employ weights that are also less than or equal to one. It remains a future challenge to incorporate negative weights for a full $[-1 \ldots 1]$ range.

We illustrate an example of multiplication by acetylation of phenol, $A_1$, and 2,6-dimethylphenol, $A_2$, with acetic anhydride, $W$, to yield phenyl acetate, $B_1$, and 2,6-dimethylphenyl acetate, $B_2$, respectively (figure 3, bottom). Equations (2.2*a*) and (2.2*b*) represent this reaction where phenols are the multiplicands and acetic anhydride is the multiplier. To accomplish this proof of concept study, phenol and acetic anhydride stock solutions were prepared at 0.1 mM in dichloromethane (DCM). Phenol stock solutions included addition of 10% pyridine to aid in solubilization of the reagents. Appropriate volumes of phenol and acetic anhydride stock solutions were aliquoted into a vial based on the stoichiometric equations (table 1, column 1). A stoichiometric equivalent of 0.1 translated to addition of 0.1 ml of the respective stock solution. In these experiments, phenols, $A_1$ and $A_2$, were first added in volumes of 0.3–0.7 ml, which corresponds to initial concentrations of 15–40 uM. Acetic anhydride was then added to the vials in volumes of 0.5–1 ml, which corresponds to concentrations of 33 to 50 uM. A final reaction volume of 1.5–2.0 ml resulted depending on the stoichiometric equivalents of phenols and acetic anhydride. The acetylation reaction and multiplication occurred as the vials were incubated on a rotary shaker at room temperature for a period of 24 h.

Concentrations of the remaining, unreacted phenol reactants, $[A_1]$ and $[A_2]$, and phenyl acetate products, $[B_1]$ and $[B_2]$, were determined by GC-MS analysis for acetylation reactions that involved various stoichiometric ratios of $W$, $A_1$ and $A_2$. GC-MS sample preparation was performed through removal of an aliquot of 0.1 ml from each reaction vial and subsequent dilution with 1.4 ml of DCM to achieve a total volume of 1.5 ml. A volume of 1 ul of these samples was injected into the GC-MS for analysis using a 15-minute temperature ramping programme from 60°C to 280°C with an initial hold of 2 min and an increase of 20°C per minute. Identification and quantitation of phenols and phenyl acetates was performed by MS using a mass selective detector (MSD) with GC/MSD MassHunter Acquisition software. The chromatograms were processed using both MassHunter and Classic ChemStation Data Analysis.

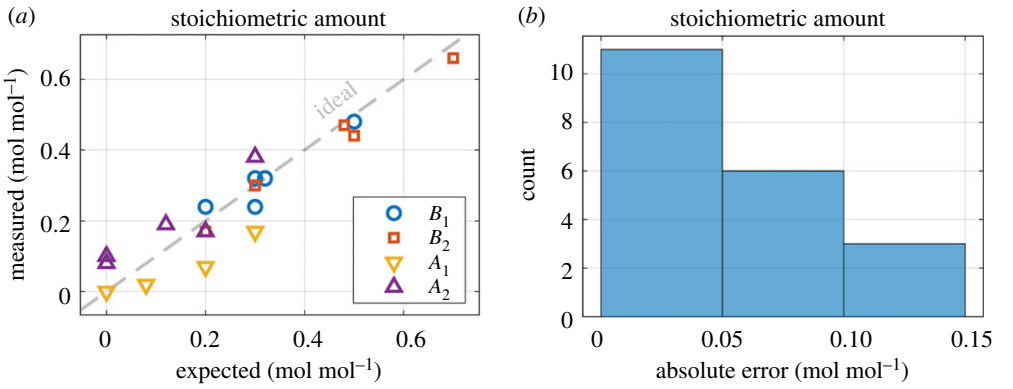


**Figure 4.** Error analysis of reaction-based multiplication. (*a*) Expected and measured concentrations of remaining, unreacted phenols, $[A_1]$ and $[A_2]$, and their respective phenyl acetate products, $[B_1]$ and $[B_2]$, are shown in the form of a scatter plot using stoichiometric equivalents as a measure of concentration. (*b*) A histogram of absolute experimental errors is also displayed, with error again shown in units of stoichiometric equivalents. (Online version in colour.)

The resulting raw GC peak areas, or abundance, of unreacted phenols and phenyl acetates was used to calculate their respective measured stoichiometric equivalents (electronic supplementary material, table S4). These stoichiometric coefficients are mole ratios of the relative amounts of reactants and products in a chemical reaction. We use these experimentally observed mole ratios as measures of concentration. Both expected and measured stoichiometric equivalents are shown for the unreacted phenols and phenyl acetates that were detected after the acetylation reaction was complete (table 1, columns 2–5).

To minimize errors from the reaction-based multiplication, incubation times were increased beyond what is typical for an acetylation reaction to ensure reaction completion. Additionally, acetic anhydride was added with enough excess so that various phenols would act as limiting reagents as opposed to the acetylating reagent. This approach does not adversely affect multiplication or formation of phenyl acetates. Consequently, two parallel acetylation reactions occurred. Relative and absolute errors were determined for this experiment. Relative error can be determined based upon a scatter plot that displays the linear correlation between expected and measured stoichiometric equivalents of the unreacted phenols and phenyl acetate products (figure 4*a*). Absolute error is shown as a histogram and also uses units of stoichiometric equivalents (figure 4*b*).

In general, average per cent error in concentration for the phenyl acetates, $B_1$ and $B_2$, was found to be 8.54% with a standard deviation of 7.71%. Absolute error was calculated at 0.028 stoichiometric equivalents with a standard deviation of 0.022 equivalents. Therefore, concentrations of phenyl acetate products, $[B_1]$ and $[B_2]$, which represent multiplication products, were found to be highly accurate and within tolerable errors of their expected values.

## (c) Addition by pooling

The previously described acetylation reaction performs multiplication; however, to perform matrix arithmetic, we need both multiplications and additions. Similar to the multiplication operations, the addition operations can also be performed *in situ*. The premise behind chemical addition is described in our previous work [16], where we show that the mixing of $N$ chemical solutions results in the volume-weighted addition of their respective initial concentrations ($[B]_n$):

$$[B]_f = \sum_{n=1}^{N} \frac{V_0}{V_f}[B]_n. \tag{2.4}$$

However, here, we transfer equal aliquots ($V_O$) from each of $N$ wells into the pool, resulting in a total volume of $N \times V_O$ and a final concentration that is proportional to the sum of all initial concentrations. The pooling of acetylation reaction mixtures into one vial represents addition. We use this to quantify the concentrations of phenyl acetates after acetylation-based multiplication without further volumetric manipulation. In preliminary experiments, this concept was evaluated using equal aliquots of 1 : 1 stoichiometric reactions of various substituted phenols and the auxiliary phenol with acetic anhydride and pooling of the resulting phenyl acetate products (electronic supplementary material, table S3).

### (d) Parallel multiply and accumulate

Multiplication with acetylation and addition by pooling are used to perform many multiply-accumulate (MAC) operations *in situ*. In a container or vial, each phenol compound represents a different data point (i.e. pixel intensity). Upon addition of acetic anhydride to mixtures of phenols, parallel acetylation reactions occur. With each vial containing a stable mixture of $M$ different phenol compounds, $A_1$, $A_2$, ... $A_M$, it is possible to represent $P$ partitions of data in equal sizes using an array of $M$ vials. The resulting chemical solution represents all $P$ data arrays simultaneously. Addition of an auxiliary compound as a complement is then performed to implement exact multiplication on these mixed chemical batches. Acetic anhydride is then added to each vial where the initial concentration of acetic anhydride added to a specific vial is analogous to the coefficient that is employed as a multiplier for the corresponding image pixel. As the rates of $M+1$ reactions are similar, this reagent will react with all phenol compounds in the chemical mixture. The resulting concentrations of phenyl acetate products, $[B_1]$, $[B_2]$, ... $[B_M]$, represent the product of the common coefficient or reactant, $[W]_o$, and the initial reactant concentrations, $[A_1]_o$, $[A_2]_o$, ..., $[A_M]_o$, respectively. An appropriate set of phenol compounds was selected based on the criteria below:

1) Phenol compounds must be stable, inert, and have no cross-reactivity with one another to allow simultaneous reactions or parallel computations.
2) Each phenol must undergo acetylation by acetic anhydride to completion, so as not to adversely affect reaction-based multiplication.
3) Phenols must react with similar kinetic profiles to eliminate potential bias toward the preferential formation of a particular phenyl acetate product.
4) Phenols must exhibit these characteristics in the proposed reaction solvent system and be compatible with automated liquid handling systems.

If these conditions are met, equal division of the acetylating reagent among all mixed phenol compounds is ensured. This ultimately allows for accurate and parallel reaction-based multiplications.

## 3. Case studies in chemical-based image processing

Digital image processing typically involves a set of convolution operations which are performed on the input image, section by section, until the entire image is processed. At each convolution step, weighted summation is performed using the weights of a coefficient matrix known as the kernel. The resulting value from one kernel position represents the corresponding output image pixel from that section of the input image. The formulation of image processing convolution for each step is presented below, where $[A](i,j)$ represents the intensity of the pixel, or concentration of the respective phenol, in location $(i,j)$ in the input image, $[W](k,l)$ denotes the kernel weight or acetic anhydride concentration applied in location $(k,l)$ in the $K \times L$ kernel, and $[B](i,j)$ is the pixel

intensity or phenyl acetate concentration in location $(i,j)$ of the output image:

$$[B](i,j) = \sum_{k=-K/2}^{K/2} \sum_{l=-L/2}^{L/2} [A](i+k, j+l) \times [W](k,l), \tag{3.1}$$

Under this premise, the operations required to perform a convolution are multiplication and addition. Thus, the chemical MAC operations presented in the 'Parallel Multiply and Accumulate' section can be used to carry out this operation.

The convolution kernel, or image filter, determines the values to be multiplied by input image pixels. In our demonstrations, a $2 \times 2$-pixel averaging kernel and a $3 \times 3$-pixel Gaussian kernel were implemented. An averaging kernel, composed of values with the same weight, was used in our first case study resulting in image smoothing from uniform pixel averaging across the image. The Gaussian kernel, composed of values with various weights, was used in the second case study resulting in radial smoothing across the image.

## (a) Case study A: using non-parallel averaging kernel

In the first case study, we perform reaction-based image processing without the use of parallel MAC operations, i.e. in our case, $M = 1$ and $Q = 16$, where $Q$ denotes the number of concentration levels. This case study was conducted to examine the feasibility of our approach prior to implementing parallel computation with multiple phenols and acetylation reactions. An averaging kernel, with identical values and weights, was employed as a convolution filter for simplicity.

A $4 \times 4$-pixel greyscale image of a gradient is encoded by various concentrations of 2,6-dimethylphenol, $[A_2]$, where the concentration of $[A_2]$ represents pixel intensity, and the concentration of the auxiliary compound, phenol, $[A_1]$, is used to ensure accurate arithmetic. In this demonstration, the greyscale image was composed of 16concentration levels, or pixel intensity values. The concentrations of $[A_1]$ and $[A_2]$ ranged from 0.05 µM to 60 µM which results in pixel intensity levels of approximately 4 µM. Each input image pixel was represented by a 1.5 mL vial and contained the two phenols, phenol, $A_1$, and 2,6-dimethylphenol, $A_2$. Stock solutions of $A_1$ and $A_2$ were prepared at 0.1 mM in DCM and 10% pyridine as diluent. Concentrations of phenols corresponding to the stoichiometric equivalents (electronic supplementary material, figure S1) were added manually in volumes of 0–0.75 ml to prepare the input image. This resulted in a total volume of 0.75 ml in each input image vial after addition of $A_1$ and $A_2$. Application of a $2 \times 2$-pixel averaging kernel to the encoded image was performed through addition of acetic anhydride, where the concentration added was equal to the kernel coefficient, $[W]$, of the corresponding input image pixel. Stock solutions of acetic anhydride were prepared at 0.1 mM in DCM and 0.25 ml was added to each input image vial for a total reaction volume of 1.0 ml. This corresponds to an addition of 25 µM of acetic anhydride and represents application of a kernel coefficient of 0.25. The vials were then placed onto a rotary shaker and allowed to react at room temperature for 24 h. Multiplication of the input image pixel by the averaging kernel occurred as the acetylation reaction proceeded forming the products, phenyl acetate, $B_1$, and 2,6-dimethylphenyl acetate, $B_2$. Addition was realized through pooling of equal aliquots from the reaction mixtures for the vials associated with each kernel position. Accordingly, aliquots of 25 ul were removed from processed input image vials and added to a new vial containing 1.4 ml of DCM for a total volume of 1.5 ml, which represents an output image pixel. This procedure was repeated for all kernel positions, or movements, across the $4 \times 4$-pixel greyscale input image. Prior to analysis, 1 µl aliquots of the output image pixel vials were removed and diluted with 1.5 ml of tetrahydrofuran (THF). The vials that compose the $3 \times 3$-pixel output image were analysed by GC-MS through injection of 1 µl of the prepared samples. The same temperature programme and analysis software described in the 'Multiplication with Acetylation' section were employed. The resulting raw GC peak areas were used to calculate the measured stoichiometric equivalents, or concentrations, of the substituted phenyl acetate product,

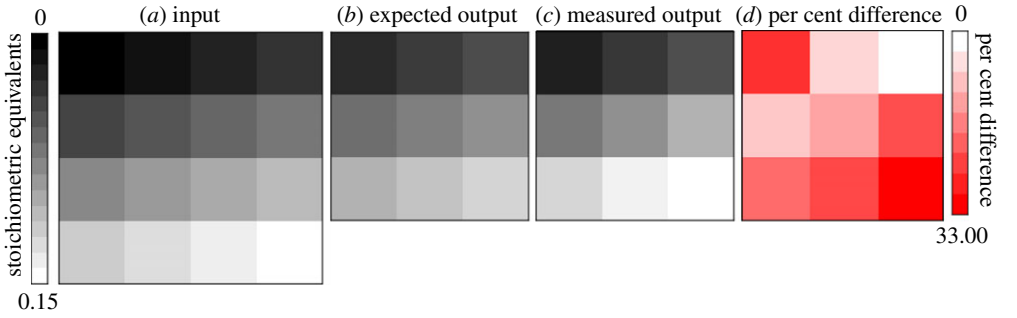


**Figure 5.** Reconstruction of a small greyscale image after image processing. A greyscale image of a gradient was processed with acetylation. The pixel intensity is shown for a range of 0 to 0.15 stoichiometric equivalents for phenols and phenyl acetates on the far left. Darker intensity pixels are represented by fewer stoichiometric equivalents and lighter intensity pixels represent more stoichiometric equivalents. (*a*) The input image of a 4 × 4-pixel greyscale gradient, where pixel intensity represents 2,6-dimethylphenol, $[A_2]$, concentration. (*b*) The 3 × 3-pixel expected output image, where pixel intensity represents expected 2,6-dimethylphenyl acetate, $[B_2]$, concentration. (*c*) The 3 × 3-pixel measured output image from implementation of the 2 × 2-pixel averaging kernel via phenol acetylation reactions, where pixel intensity is determined from GC-MS analysis and the resulting 2,6-dimethylphenyl acetate, $[B_2]$, concentrations. (*d*) The per cent difference between expected and measured output images, where white indicates low per cent difference and red indicates higher per cent difference corresponding to the scale on the far right. (Online version in colour.)

$[B_2]$, which corresponds to the output image pixel intensity. The processed output image was reconstructed based on these measurements *in silico*. An overview of this method can be seen in figure 1 in the 'Introduction' section.

Expected concentrations of phenyl acetates for the output image have been calculated based on conserved stoichiometry. Measured concentrations of phenyl acetates were obtained as raw GC peak areas from GC-MS analysis. These areas were converted to stoichiometric equivalents, or mole ratios, which were then compared to the expected values (electronic supplementary material, table S5). The expected input image was generated *in silico* based on expected stoichiometric equivalents of 2,6-dimethylphenol, $[A_2]$ (figure 5*a*). The expected output image was based on expected stoichiometric equivalents of 2,6-dimethylphenyl acetate, $[B_2]$ (figure 5*b*). The measured output image was also reconstructed *in silico* using the measured concentrations obtained through GC-MS of 2,6-dimethylphenyl acetate, $[B_2]$ (figure 5*c*). Per cent difference between the expected and measured output images was then calculated (figure 5*d*), where per cent difference ranged from 2.08 to 32.72% with an average per cent difference of 17.58%.

The measured concentration of 2,6-dimethylphenyl acetate, $[B_2]$, was converted from raw GC peak areas to mole ratios and assessed in stoichiometric equivalents to determine error in our reaction-based image processing approach. Relative error in concentration can be determined based upon a scatter plot that displays the linear correlation between expected and measured stoichiometric equivalents of phenyl acetate, $[B_1]$, and 2,6-dimethylphenyl acetate, $[B_2]$ (figure 6*a*). Absolute error in concentration is shown in the form of a histogram, also in units of stoichiometric equivalents (figure 6*b*). Overall, the average per cent error per pixel was determined to be 24.89% with a standard deviation of 14.98%. The average absolute error was found to be 0.036 stoichiometric equivalents with a standard deviation of 0.025 equivalents.

## (b) Case study B: using parallel Gaussian kernel

The second reaction-based multiplication demonstration involves the use of simultaneous MAC operations performed by parallel acetylation reactions, i.e. $M = 4$, $Q = 8$. With this approach, a greyscale image of a plus sign is effectively blurred using a Gaussian kernel. Gaussian filters are the most widely used smoothing filters and are frequently employed in image enhancement. In contrast to uniform pixel averaging or image blurring, this filter blurs the input image in a radial

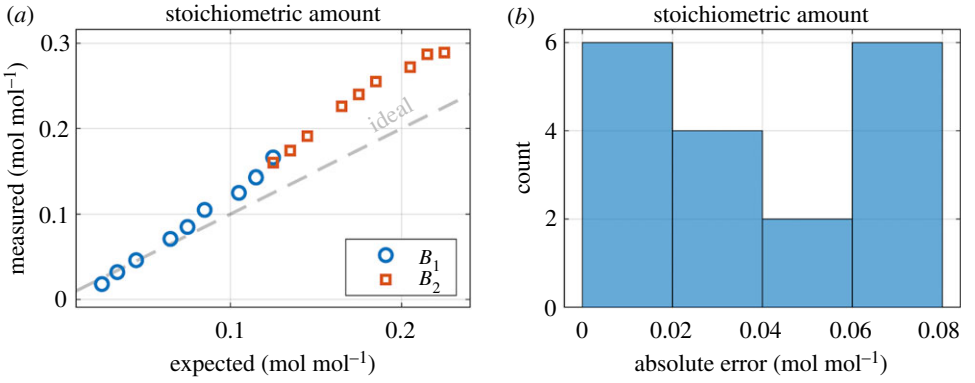


**Figure 6.** Error analysis of image processing case study. (*a*) Expected and measured amounts of phenyl acetate, [$B_1$] and 2,6-dimethylphenyl acetate, [$B_2$], are shown in the form of a scatter plot using stoichiometric equivalents. (*b*) A histogram of absolute experimental errors in phenyl acetate concentration is also displayed, with error again shown in units of stoichiometric equivalents. (Online version in colour.)

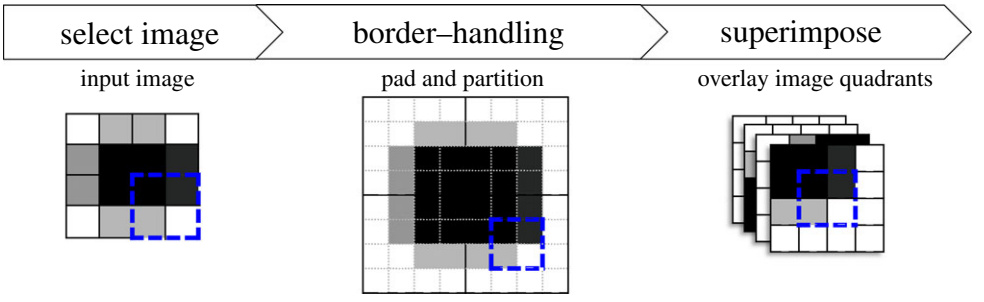


**Figure 7.** Preparation of a greyscale image for parallel image processing. This scheme shows the selected 4 × 4-pixel greyscale input image of an asymmetric plus sign (left). The input image is then padded and partitioned prior to encoding in phenol compounds to create an 8 × 8-pixel input image (middle). This practice ensures accurate processing of pixels located along the borders of the image partitions. The four 4 × 4-pixel image quadrants are then superimposed to allow parallel processing of the four image quadrants (right). The dashed blue box is shown in each of the three preparation steps and highlights the lower right quadrant of the original input image as it is padded, partitioned and superimposed. (Online version in colour.)

fashion. Important use cases of this kernel include noise suppression and feature extraction [22]. Additionally, a lack of negative weights make this image filter an attractive option for exploring the area of chemical computation.

We implement a zero padding and partitioning technique that allows parallel processing of image partitions simultaneously. In our demonstration, the 4 × 4-pixel greyscale input image is padded to account for the processing of image borders, or boundaries, between image partitions. This results in a padded 8 × 8-pixel input image, which is then divided into four 4 × 4-pixel quadrants (figure 7).

Each image quadrant is represented by a different substituted phenol, o-cresol, $A_3$, p-cresol, $A_4$, p-propylphenol, $A_5$ and, p-tert-butylphenol, $A_6$, and thus, can be superimposed. Parallel acetylation reactions occur with these phenols upon addition of acetic anhydride resulting in parallel computation at four times the standard throughput (figure 8).

To apply a Gaussian kernel to a chemically encoded greyscale image, a simple addition of a concentration of acetic anhydride equal to the kernel coefficient of the corresponding chemical input pixel is performed. As such, the utilization of the image processing smoothing filters suits both our computing purposes and experimental design. To further simplify the process of applying kernel weights chemically using standard resolution pipettes, the values of the kernel

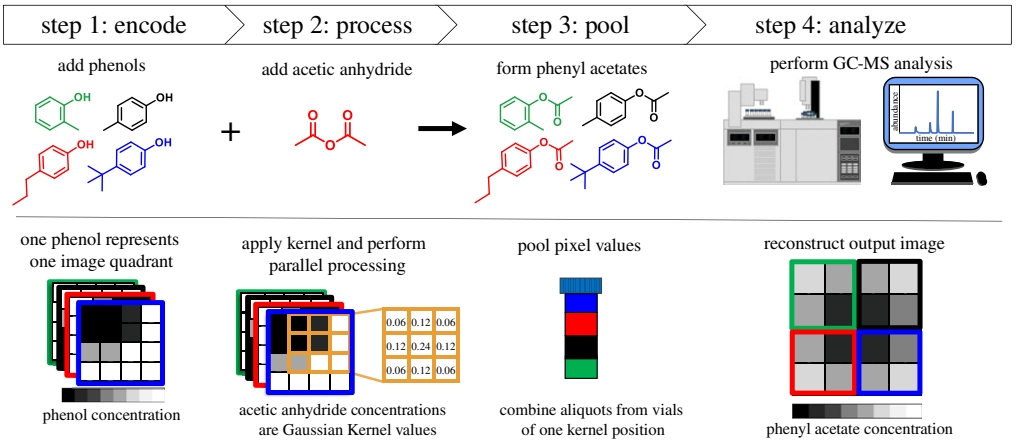


**Figure 8.** Overview of parallel image processing using chemical reactions. This scheme shows the workflow for parallel image processing using chemical reactions which involves mixtures of phenol compounds and simultaneous phenol acetylation. In step 1, the 4 × 4- pixel superimposed image quadrants of the padded and partitioned 8 × 8-pixel input image are encoded using various concentrations of phenols. Darker pixel intensity corresponds to lower concentrations of phenols and lighter pixel intensity corresponds to higher concentrations of phenols. Each phenol represents one quarter of the image by o-cresol (green), p-cresol (black), p-propylphenol (red) and p-tert-butylphenol (blue). The auxiliary compound, phenol, is not shown here as it is used as a complement to ensure exact arithmetic. The four 4 × 4-pixel image quadrants are superimposed through chemical mixtures of phenols in one vial or input image pixel. In step 2, the 3 × 3-pixel Gaussian kernel, shown in the orange box, is applied one position at a time through acetic anhydride addition for simulation of image processing via a convolution filter. In step 3, equal aliquots of the resulting phenyl acetates, o-tolyl acetate (green), m-tolyl acetate (black), p-propylphenyl acetate (red) and p-tert-butylphenyl acetate (blue), are pooled from the input image vials associated with each kernel position into a new vial representing an output image pixel of the superimposed image quadrants. In step 4, these vials are analysed using the GC-MS to obtain the output image pixel intensity which is represented by the phenyl acetate concentration. The output image is then reconstructed *in silico* from the values of phenyl acetates measured during analysis and superimposed image sections are separated with each phenyl acetate representing one image quadrant. (Online version in colour.)

matrix are approximated before implementation. In Gaussian kernels, this practice leads to subtle changes in the kernel matrix such that the kernel does not sum to 1. Convolution filters used in image processing for blurring should equal 1 as this maintains the mean of the image values. Therefore, all experimentally obtained values are normalized to the overall value of the kernel, which in our experiments is 0.96. Parallel computation is achieved when the phenol acetylation reactions are complete.

The encoded input image data is first written to vial cassettes with various concentrations of phenols, $[A_3]$, $[A_4]$, $[A_5]$ and $[A_6]$, using liquid handling robotics. The superimposed input image pixels were each represented by a 1.5 ml vial that contained the four phenols, where each phenol depicts a different input image quadrant. In this demonstration, the greyscale input image was composed of 8 concentration levels, or pixel intensity values. The concentrations of $[A_3]$, $[A_4]$, $[A_5]$ and $[A_6]$ ranged from 270 to 530 uM which results in pixel intensity levels of approximately 40 µM. These concentration levels may seem arbitrary, however, this range translates to volumetric transfers in amounts of 0.1 to 0.2 ml. When this volume range is divided into 8 equal levels, each 14 ul increment corresponds to a pixel intensity level of approximately 40 µM. This was done to simplify image encoding performed by a liquid handling robot. All stock solutions of phenols were prepared at 4M concentration in propionitrile with 10% pyridine. First the phenols, $A_3$, $A_4$, $A_5$ and $A_6$ were added to each overlaid input image vial in amounts of 0.1–0.2 ml. The auxiliary compound, $A_1$, was added last to allow all input image vials to contain 0.8 ml in total volume. Image processing by kernel application via acetic anhydride addition was then performed manually. A 3 × 3-pixel Gaussian kernel was used with each vial cassette

containing 6 kernel positions composed of 9 Gaussian kernel weights, [$W$], for a total of 54 vials per cassette. The 9 Gaussian weights consisted of repeating weighted values of 0.24, 0.12 and 0.06 (figure 8, step 2). Three comparable acetic anhydride stock solutions were prepared to simulate these weighted kernel values at 7.74, 3.89 and 1.93 M in propionitrile and correspond to kernel weights of 0.24, 0.12 and 0.06, respectively. The appropriate acetic anhydride stock solutions were added in amounts of 0.2 ml to each overlaid input image pixel vial resulting in a final reaction volume of 1.0 ml for all vials. The entire vial cassette was then placed on a rotary shaker and the acetylation reactions proceeded at room temperature over the course of 24 h. All four phenols that represent the input image data ($A_3$, $A_4$, $A_5$ and $A_6$) in each vial undergo simultaneous acetylation resulting in the formation of o-tolyl acetate, $B_3$, m-tolyl acetate, $B_4$, p-propylphenyl acetate, $B_5$, and p-tert-butylphenyl acetate, $B_6$ and parallel reaction-based multiplication.

Pooling of equal volumetric fractions from vials of one kernel position into a new vial representing the output image pixel was then performed to represent addition in the MAC operations. A 10 µl aliquot of each input image vial in one kernel position was pooled into a new vial containing 1.41 ml of THF for a total volume of 1.5 ml. This procedure is repeated for each kernel position, or movement, until the entire processed input image has been pooled into respective output image vials. This resulted in a $2 \times 2$-pixel output image composed of four overlaid $2 \times 2$-pixel image quadrants (electronic supplementary material, figure S2). Prior to analysis, an inert internal standard was added to each output image vial to normalize the measurements and account for instrumental variation. A stock solution of butylated hydroxytoluene (BHT) was prepared at a concentration of 0.1 M in propionitrile. A working solution was then prepared by diluting this stock using THF to a concentration of 266 µM. A 1 : 10 dilution of the output image vials was performed with this working solution allowing the final concentration of BHT in the GC-MS samples to be 239 µM. Output image vials containing the internal standard were then analysed by GC-MS (electronic supplementary material, figure S3) through injection of 1 µl of these solutions. The same temperature programme and analysis software described in the 'Multiplication with Acetylation' section were employed. The resulting raw GC peak areas for each phenyl acetate were compared to calibration curves (electronic supplementary material, figure S4 and table S7) to determine phenyl acetate concentration for [$B_3$], [$B_4$], [$B_5$] and [$B_6$], or output image pixel intensity. The image partitions were then separated and reconstructed based on concentration, or intensity levels, *in silico* to form the final $4 \times 4$-pixel output image. Raw GC peak area, or abundance, was used to calculate the concentration of phenyl acetates, which was then converted to stoichiometric ratios (electronic supplementary material, table S6).

The expected input image and output image were generated *in silico* based on expected stoichiometric equivalents of substituted phenols, [$A_3$], [$A_4$], [$A_5$] and [$A_6$] (figure 9*a*), and their phenyl acetate products, [$B_3$], [$B_4$], [$B_5$] and [$B_6$] (figure 9*b*), respectively. The output image for this case study was also reconstructed *in silico* using the measured concentrations of substituted phenyl acetates, [$B_3$], [$B_4$], [$B_5$] and [$B_6$] (figure 9*c*). Per cent difference between the expected and measured output images was then calculated (figure 9*d*), where per cent difference ranged from 0.41 to 25.64% with an average per cent difference of 6.56%.

Errors were evaluated when performing reaction-based multiplication for parallel computation. The measured concentrations of the phenyl acetates, [$B_3$], [$B_4$], [$B_5$] and [$B_6$], obtained by GC-MS were assessed in stoichiometric equivalents to reconstruct the measured output image. Additionally, an internal standard, BHT, was added to each vial prior to GC-MS analysis in a fixed concentration to allow normalization of phenyl acetate peak areas and instrumental response. This practice accounts for errors due to instrumental variability during analysis of samples assessed on the same day (intra-) and on different days (inter-). Relative error in concentration can be determined as a scatter plot that compares the experimental measurements of phenyl acetates, [$B_3$], [$B_4$], [$B_5$] and [$B_6$], to the expected values and is shown with stoichiometric equivalents (figure 10*a*). Absolute error in concentration is shown in the form of a histogram, also in units of stoichiometric equivalents (figure 10*b*). In general, the average per cent error per pixel was calculated at 6.35% with a standard deviation of 6.57%. The average

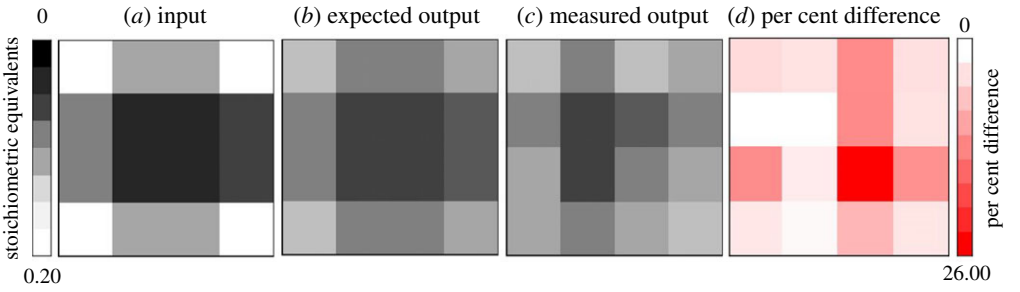


Q2 **Figure 9.** Reconstruction of a small greyscale image after parallel image processing. A 4 × 4-pixel greyscale image of an asymmetric plus sign was processed with acetylation. The image was padded to form an 8 × 8-pixel input image which was then partitioned into four 4 × 4-pixel quadrants that were superimposed and is not shown here. The pixel intensity is shown on the far left for a range of 0 to 0.20 stoichiometric equivalents for phenols and phenyl acetates. Darker intensity pixels are represented by fewer stoichiometric equivalents. Conversely, lighter intensity pixels represent more stoichiometric equivalents. (*a*) The 4 × 4-pixel expected input image, where pixel intensity represents phenol concentration. Each 2 × 2-pixel quadrant represents a different substituted phenol, [$A_3$], [$A_4$], [$A_5$] and [$A_6$]. (*b*) The 4 × 4-pixel expected output image, where pixel intensity represents expected phenyl acetate concentration. Each 2 × 2-pixel quadrant represents a different substituted phenyl acetate, [$B_3$], [$B_4$], [$B_5$] and [$B_6$]. (*c*) The 4 × 4-pixel measured output image from implementation of the 3 × 3-pixel Gaussian kernel via phenol acetylation reactions, where pixel intensity is determined from GC-MS analysis and the resulting phenyl acetate concentrations, [$B_3$], [$B_4$], [$B_5$] and [$B_6$]. (*d*) The per cent difference between expected and measured output images, where white indicates low per cent difference and red indicates higher per cent difference corresponding to the scale on the far right. (Online version in colour.)

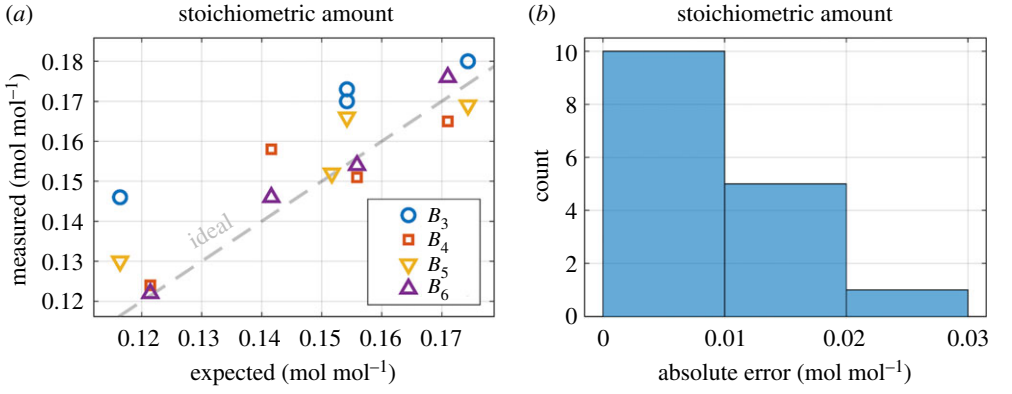


**Figure 10.** Error analysis of parallel image processing case study. (*a*) Expected and measured amounts of phenyl acetates, [$B_3$], [$B_4$], [$B_5$] and [$B_6$], are shown in the form of a scatter plot using stoichiometric equivalents. (*b*) A histogram of absolute experimental errors is also displayed for all phenyl acetate concentrations, with error again shown in units of stoichiometric equivalents. (Online version in colour.)

absolute error was found to be 0.008 stoichiometric equivalents with a standard deviation of 0.008 equivalents. These values were much improved from the first image processing case study and show use of fewer concentration, or pixel intensity, levels and inclusion of experimental controls, such as internal standards, can improve reaction-based chemical computing.

## 4. Discussion

In this work, we propose the use of the acetylation reaction to perform the matrix multiplications involved in image processing. Our reaction-based processing approach has advantages over

other demonstrations of information processing by chemicals. Most of these studies involve oscillating reactions, and are used in applications for memory and pattern recognition. Reported efforts have successfully shown that chemical computers are programmable and can perform complex classification while tolerating high levels of noise. However, many of these experiments involve oscillator-based computing which is limited by weak interactions, development of non-synchronous phases and narrow windows of computational readout with no clear beginning or end to the reaction [23,24]. The reaction–diffusion processes associated with these computations can also require the use of droplets, where size and composition must be controlled [25]. Although microfluidic devices could improve these experiments, the related techniques are difficult and more demanding than the acetylation reaction employed in this work. In comparison, we adopt a more practical approach that uses chemical reactions to implement the multiplication operation on many chemical species. Additionally, several levels of concentration are used to represent multi-bit storage per vial, which allows for higher resolution computation. This is an improvement over our previous work which uses binary concentration levels and performs multiplication and weighted summation by volumetric fractions of non-reactive chemical solutions for image classification [16]. Notably, we use a fundamental chemical reaction and straightforward experimental set-up for computing multiplications and additions. The demonstrations presented here expand upon current applications of computing with chemical mixtures and suggest acetylation reactions as a more easily attainable option for chemical information processing. Both phenols and their phenyl acetate products can be used as inputs in subsequent chemical transformations, which could allow development of multi-layered chemical circuits [26–29]. Additionally, acetylation is familiar to most chemists for the protection of functional groups [30] and is important in cellular biology for the modification of proteins [31].

Although we have presented a practical application for chemical computing, several limitations of our approach exist. Various sources of error were identified and largely attributed to the manual dispensing or automated dispensing by liquid handling equipment and the analytical instrumentation adopted for this work, rather than the reaction-based multiplication. Small volumes of phenol stock solutions were dispensed manually or by an automated pipetting robot using standard resolution pipettes to encode input images. Manual pipetting led to an average of approximately 6% error per input image pixel, whereas automated pipetting was determined to have an average approximately 4% error per pixel (data not shown). Inaccuracies with these measurements were propagated throughout the demonstration. Ultimately, these errors impacted the amounts of phenyl acetates formed and subsequent reconstruction of output images via instrumental analysis. We use the GC-MS for detection and quantitation of the phenyl acetate multiplication products. However, the GC-MS is constrained in its ability to differentiate among the narrow pixel intensity levels chosen for our case studies. The analytic and quantitative power of the GC-MS does not always extend to such limited concentration ranges. The combined effect of the limitations of the equipment and analytical instrumentation results in moderate errors with output pixel measurement. However, we have addressed these experimental issues as is evidenced by the decrease in error between the two image processing case studies. In this work, we observed approximately 25% error per pixel in the image processing case study involving an averaging kernel and approximately 6% error per pixel in the parallel image processing case study involving a Gaussian kernel. The former employs 16 levels of concentration or pixel intensity, that are encoded manually, while the latter uses 8 much broader levels of concentration that are encoded via automation. This practice can remedy inaccuracies associated with manual and automated dispensing and instrumental analysis. Additionally, the parallel image processing case study incorporates experimental controls, such as internal standards, and can further reduce errors from intra- and inter-day instrumental variation. This leads to more accurate phenyl acetate analysis and pixel intensity level designations with respect to output image reconstruction. There is also potential for reduction of error beyond what was attempted in our case studies. Larger deviations in the output image are noted in pixels corresponding to lower concentrations of phenyl acetates. Therefore, the concentration range of phenols used

for encoding input images could be shifted to obtain greater amounts of phenyl acetates after processing with acetic anhydride. This could improve our approach as errors introduced during manual or automated pipetting and analysis would have less impact on reconstruction of output images.

The MAC operations executed in this work via phenol acetylation and pooling represent a set of chemical computations involved in image processing. These computations can be scaled spatially with use of many vial cassettes to increase image size. Furthermore, the partitioning technique employed here allows for parallelized chemical computation resulting in additional increases to image size and computational throughput. Here, we use one vial cassette to represent a padded $8 \times 8$-pixel input image, which is partitioned into four superimposed $4 \times 4$-pixel quadrants and represented by four unique phenols. However, theoretically, a larger greyscale image, such as a padded $24 \times 24$-pixel input image, could be partitioned into four superimposed $12 \times 12$-pixel quadrants by using 18 vial cassettes and the same four phenols. This amounts to an increase in image size of threefold. Furthermore, greater numbers of phenols could be used to increase the amount of image partitions. For instance, nine different phenols can represent nine superimposed image partitions. In the aforementioned example, if each phenol represents a $12 \times 12$-pixel section of the image, this translates to an additional increase in image size and computational throughput of approximately 2-fold. The premise of synthesizing multiple products from a mixture of reagents in a single reaction is the basis of combinatorial chemistry and is frequently used to build chemical libraries containing tens of thousands of compounds [32]. Typically, the application of in solution combinatorial chemistry is limited as cross-reactivity, deconvolution, and purification of products can be problematic [33]. However, this concept is viable for our purposes as phenols are inert and only stoichiometry and kinetics would need to be examined since we are primarily concerned with formation, detection, and quantitation of products. Temporal scaling can also be decreased by as much as fourfold, considering the acetylation reaction is complete after only 6–8 h as compared to the 24-h incubation period adopted for this work. Therefore, our approach to chemical image processing can be extended both spatially and temporally beyond the demonstration implemented in this work without sacrificing accuracy.

In future undertakings, compatibility of this experimental framework with more high-throughput liquid handling robots can be investigated. For example, acoustic liquid handling instruments can perform volumetric transfers on a smaller scale and at a markedly increased rate when compared to the automated pipetting robots used during our reaction set-up. Additionally, these instruments have increased precision and accuracy since acoustic waves are used to manipulate small droplets of stock solutions. This circumvents the limitations imposed by the standard resolution pipettes our robot employs. This type of automated instrumentation can also be coupled to in-line analytics, such as with MS detectors. MS can not only identify, but also quantify amounts of phenols and phenyl acetate products without chromatographic separation, which is another limitation observed in our workflow. Even with use of the GC-MS, previous studies report detection and quantitation of 1550 chemicals in one analysis [34]. This could allow substantial increases in amounts of phenols used to encode input image data, thereby enabling many more image partitions than we have described here. Incorporation of these concepts could limit reagent consumption, costs, and time while allowing larger image processing demonstrations to be realized. As previously discussed, in solution combinatorial chemistry has the potential to generate tens of thousands of small molecules from a mixture of reagents in a single reaction. A group from Glaxo has reported synthesis and analysis of a library of amides from mixtures of 80 acid chlorides and amines [35]. To illustrate these points, there are almost 400 phenols that are commercially available. Using only a quarter of these phenols to represent image partitions could lead to an increase in image size and computational throughput of 25-fold. Although not all of these reagents would adhere to the chemical criteria required for reaction-based computation and the amounts of reagents would be nearing the reported maximums, this proposition is theoretically possible with experimental validation. Additionally, acoustic liquid handling robots, such as the Echo® series by Labcyte, can perform up to 750 000 high precision

volumetric transfers per day with lower error rates than tip-based technology. By making use of the available reagents and these robotic systems, demonstrations of chemical image processing have the potential to increase image size and computational throughput by several orders of magnitude.

Although initial attempts at chemical computation largely involve DNA-based methods [3–7], to perform these experiments, the reagents must be methodically designed and synthesized. By contrast, the reagents used in this work are commercially available and undergo a simple transformation to represent multiplication, the foundation of matrix operations. This type of *in chemico* computing can be performed under mild conditions and employs common analytical instrumentation that is familiar to most bench scientists. With these conditions in mind, we believe chemical computing involving solution-based chemical reactions is a more feasible approach. Moreover, acetylations of anilines and thiols could serve as an alternative to phenol acetylation, as these reactions are mechanistically similar and thus, could also display reaction-based multiplication [36,37]. Therefore, one of the most compelling prospects of our approach involves its potential for use with cascaded operations. The products of acetylation reactions (phenyl acetates, phenyl acetamides and phenyl thioesters) can serve as the inputs for a number of chemical transformations [27–29,38,39], which ultimately enable sequential, layered computations. In this regard, our work lays the foundations for the next generation of chemical computing systems.

## 5. Conclusion

In summary, we have shown that chemical reactions can be used to process information in the form of greyscale images. Chemical transformations, like simplistic protection group chemistries, can be exploited to perform arithmetic and be extended for use in complex computations, such as matrix multiplication. In this work, MAC operations were demonstrated by reaction-based multiplication through the phenol acetylation reaction and addition was performed by pooling, or the combination of equal aliquots of reaction mixtures. Preliminary experiments confirmed that this framework could be used to simulate the MAC operations employed for kernel-based image processing. Two small greyscale images were processed with chemical reactions applying either an averaging or Gaussian kernel in our demonstrations. With this method, output images from the two image processing case studies were reconstructed. Additionally, this work applies the phenol acetylation reaction for image processing and is the first of its kind among many examples of image classification. Furthermore, we show that reaction-based multiplication is a viable option for *in chemico* image processing. It is our hope that this premise will be expanded upon as robotic technology evolves and aid in the future development of chemical computing systems.

Data accessibility. The datasets supporting this article have been uploaded as part of the electronic supplementary material.

Authors' contributions. A.D. and K.O. helped conceive of the study, performed experiments and analysis, and participated in writing of the manuscript. C.A. and F.N. assisted with robotic instrumentation, performed analysis, and participated in writing of the manuscript. S.C. helped conceive of the study and perform experiments. B.R., C.R., J.R., S.R. and E.K., coordinated and helped conceive of this work and assisted with the manuscript revision process. All authors read and gave final approval of the manuscript and agree to be held accountable for the work performed therein.

Competing interests. We declare we have no competing interests.

Funding. This research was supported by funding from the Defense Advanced Research Projects Agency (DARPA W911NF-18-2-0031). The views, opinions, and/or findings expressed are those of the authors and should not be interpreted as representing the official views or policies of the Department of Defense or the U.S. Government. This work was also made possible by support from the Office of the Vice President for Research at Brown University, and by the National Science Foundation under grant no. 1941344.

Acknowledgements. We would like to thank Dr Eamonn Kennedy, Dr Hokkchay Tann and Ben Foulon (Brown University) and Albert Wong (University of Twente) for helpful discussions and input.

## References


1. Eigen M, de Maeyer L. 1966 Chemical means of information storage and readout in biological systems. *Sci. Nat.* **53,** 50–57. (doi:10.1007/BF00594747)
2. Grozinger L *et al.* 2019 Pathways to cellular supremacy in biocomputing. *Nat. Commun.* **10,** 1–11. (doi:10.1038/s41467-019-13232-z)
3. Zhang Z, Fan TW, Hsing IM. 2017 Integrating DNA strand displacement circuitry to the nonlinear hybridization chain reaction. *Nanoscale* **9,** 2748–2754. (doi:10.1039/c6nr06589a)
4. Cardelli L. 2010 Two-domain DNA strand displacement. *arXiv preprint*, arXiv:1006.2993. (doi:10.4204/EPTCS.26.5)
5. Schmidt KA, Henkel CV, Rozenberg G, Spaink HP. 2004 DNA computing using single-molecule hybridization detection. *Nucleic Acids Res.* **32,** 4962–4968. (doi:10.1093/nar/gkh817)
6. Frutos AG, Liu Q, Thiel AJ, Sanner AM, Condon AE, Smith LM, Corn RM. 1997 Demonstration of a word design strategy for DNA computing on surfaces. *Nucleic Acids Res.* **25,** 4748–4757. (doi:10.1093/nar/25.23.4748)
7. Song T, Eshra A, Shah S, Bui H, Fu D, Yang M, Mokhtar R, Reif J. 2019 Fast and compact DNA logic circuits based on single-stranded gates using strand-displacing polymerase. *Nat. Nanotechnol.* **14,** 1075–1081. (doi:10.1038/s41565-019-0544-5)
8. Salehi SA, Parhi KK, Riedel MD. 2017 Chemical reaction networks for computing polynomials. *ACS Synth. Biol.* **6,** 76–83. (doi:10.1021/acssynbio.5b00163)
9. Hao Y, Hu J, Wu L, Yuan C. 2001 Image processing using BZ reaction. *2001Proc. SPIE, Image Matching Anal.* **4552**, 34–39. (doi:10.1007/s11431-010-3114-5)
10. Holley J, Jahan I, Costello BDL, Bull L, Adamatzky A. 2011 Logical and arithmetic circuits in Belousov-Zhabotinsky encapsulated disks. *Phys. Rev. E* **84,** 056110. (doi:10.1103/PhysRevE.84.056110)
11. Costello BD, Adamatzky A. 2005 Experimental implementation of collision-based gates in Belousov–Zhabotinsky medium. *Chaos Soliton. Fract.* **25,** 535–544. (doi:10.1016/j.chaos.2004.11.056)
12. Cardelli L, Kwiatkowska M, Whitby M. 2018 Chemical reaction network designs for asynchronous logic circuits. *Nat. Comput.* **17,** 109–130. (doi:10.1007/s11047-017-9665-7)
13. Banzhaf W, Dittrich P, Rauhe H. 1996 Emergent computation by catalytic reactions. *Nanotechnology* **7,** 307. (doi:10.1088/0957-4484/7/4/001)
14. Andersen JL, Flamm C, Merkle D, Stadler PF. 2017 An intermediate level of abstraction for computational systems chemistry. *Phil. Trans. R. Soc. A* **375,** 20160354. (doi:10.1098/rsta.2016.0354)
15. Cardelli L, Tribastone M, Tschaikowski M. 2020. From electric circuits to chemical networks. *Nat. Comput.* **19,** 237–248. (doi:10.1007/s11047-019-09761-7)
16. Arcadia C *et al.* 2018 Parallelized linear classification with volumetric chemical perceptrons. *2018IEEE Int. Conf. Rebooting Computing (ICRC)*, 1–9. (doi:10.1109/ICRC.2018.8638627)
17. Reed MA, Tour JM. 2000 Computing with molecules. *Sci. Am.* **282,** 86–93. (doi:10.1038/scientificamerican0600-86)
18. Mukherjee S, Hao YH, Orth K. 2007 A newly discovered post-translational modification–the acetylation of serine and threonine residues. *Trends Biochem. Sci.* **32,** 210–216. (doi:10.1016/j.tibs.2007.03.007)
19. Zhao S *et al.* 2010 Regulation of cellular metabolism by protein lysine acetylation. *Science* **327,** 1000–1004. (doi:10.1126/science.1179689)
20. Fritz JS, Schenk GH. 1959 Acid-catalyzed acetylation of organic hydroxyl groups. *Anal. Chem.* **31,** 1808–1812. (doi:10.1021/ac60155a034)
21. Riordan JF, Vallee BL. 1967 Acetylation. *Methods Enzymol.* 11, 565–570. (doi:10.1016/S0076-6879(67)11068-9)
22. Deng G, Cahill LW. 1993 An adaptive Gaussian filter for noise reduction and edge detection. In 1993IEEE Conference record nuclear science Symposium and medical imaging Conference, pp. 1615–1619.
23. Vodenicarevic D, Locatelli N, Araujo FA, Grollier J, Querlioz D. 2017 A nanotechnology-ready computing scheme based on a weakly coupled oscillator network. *Sci. Rep.* **7,** 44772. (doi:10.1038/srep44772)
24. Parrilla-Gutierrez JM, Sharma A, Tsuda S, Cooper GJ, Aragon-Camarasa G, Donkers K, Cronin L. 2020 A programmable chemical computer with memory and pattern recognition. *Nat. Commun.* **11,** 1–8. (doi:10.1038/s41467-020-15190-3)

25. Gorecki J, Gizynski K, Guzowski J, Gorecka JN, Garstecki P, Gruenert G, Dittrich P. 2015 Chemical computing with reaction–diffusion processes. *Phil. Trans. R. Soc. A* **373,** 20140219. (doi:10.1098/rsta.2014.0219)
26. El Kaïm L, Grimaud L. 2010 Ugi–Smiles couplings: new entries to N-aryl carboxamide derivatives. *Mol. Divers.* **14,** 855–867. (doi:10.1007/s11030-009-9175-3)
27. Yamazaki J, Watanabe T, Tanaka K. 2001 Enantioselective synthesis of allenecarboxylates from phenyl acetates through C-C bond forming reactions. *Tetrahedron: Asymmetry* **12,** 669–675. (doi:10.1016/S0957-4166(01)00114-8)
28. Biscoe MR, Buchwald SL. 2009 Selective monoarylation of acetate esters and aryl methyl ketones using aryl chlorides. *Org. Lett.* **11,** 1773–1775. (doi:10.1021/ol900295u)
29. Bruice TC, Donzel A, Huffman RW, Butler AR. 1967 Aminolysis of phenyl acetates in aqueous solutions. VII. 1Observations on the influence of salts, amine structure, and base strength. *J. Am. Chem. Soc.* **89,** 2106–2121. (doi:10.1021/ja00953a020)
30. Olofson RA, Kendall RV. 1970 Protection by acylation in the selective alkylation of heterocycles. *J. Org. Chem.* **35,** 2246–2248. (doi:10.1021/jo00832a031)
31. Christensen DG, Baumgartner JT, Xie X, Jew KM, Basisty N, Schilling B, Kuhn ML, Wolfe AJ. 2019 Mechanisms, detection, and relevance of protein acetylation in prokaryotes. *MBio* **10,** e02708-18. (doi:10.1128/mBio.02708-18)
32. Carell T, Wintner EA, Sutherland AJ, Rebek Jr J, Dunayevskiy YM, Vouros P. 1995 New promise in combinatorial chemistry: synthesis, characterization, and screening of small-molecule libraries in solution. *Chem. Biol.* **2,** 171–183. (doi:10.1016/1074-5521(95)90072-1)
33. Van Hijfte L, Marciniak G, Froloff N. 1999 Combinatorial chemistry, automation and molecular diversity: new trends in the pharmaceutical industry. *J. Chromatogr. B Biomed. Sci. Appl.* **725,** 3–15. (doi:10.1016/S0378-4347(99)00007-9)
34. Bergmann AJ, Scott RP, Wilson G, Anderson KA. 2018 Development of quantitative screen for 1550chemicals with GC-MS. *Anal. Bioanal. Chem.* **410,** 3101–3110. (doi:10.1007/s00216-018-0997-7)
35. Rasheed A, Farhat R. 2013 Combinatorial chemistry: a review. *Int. J. Pharm. Sci.* **4,** 2502. (doi:10.13040/IJPSR.0975-8232.4(7).2502-16)
36. Prasad HS, Srinivasa GR, Channe Gowda D. 2005 Convenient, cost-effective, and mild method for the N-acetylation of anilines and secondary amines. *Synth. Commun.* **35,** 1189–1195. (doi:10.1081/SCC-200054764)
37. Ranu BC, Dey SS, Hajra A. 2003 Highly efficient acylation of alcohols, amines and thiols under solvent-free and catalyst-free conditions. *Green Chem.* **5,** 44–46. (doi:10.1039/B211238H)
38. Li X, Wang J, Xie X, Dai W, Han X, Chen K, Liu H. 2020 Ir (iii)-Catalyzed direct C–H functionalization of N-phenylacetamide with α-diazo quinones: a novel strategy for producing 2-hydroxy-2′-amino-1, 2′-biaryl scaffolds. *Chem. Commun.* **56,** 3441–3444. (doi:10.1039/C9CC08297B)
39. Park N, Park K, Jang M, Lee S. 2011 One-pot synthesis of symmetrical and unsymmetrical aryl sulfides by Pd-catalyzed couplings of aryl halides and thioacetates. *J. Org. Chem.* **76,** 4371–4378. (doi:10.1021/jo2007253)